THE JOURNAL OF BIOLOGICAL CHEMISTRY VOL. 285, NO. 14, pp. 11023–11030, April 2, 2010
Printed in the U.S.A.

Loss of Dact1 Disrupts Planar Cell Polarity Signaling by Altering Dishevelled Activity and Leads to Posterior Malformation in Mice*

Received for publication, November 15, 2009, and in revised form, February 8, 2010 Published, JBC Papers in Press, February 9, 2010, DOI 10.1074/jbc.M109.085381

Jun Wen[‡1], Y. Jeffrey Chiang[§1], Chan Gao[‡], Hua Xue[‡], Jingyue Xu[¶], Yuanheng Ning[‡], Richard J. Hodes[§‖], Xiang Gao[¶], and Ye-Guang Chen[‡2]

From the [‡]State Key Laboratory of Biomembrane and Membrane Biotechnology, College of Life Sciences, Tsinghua University, Beijing 100084, China, the [§]Experimental Immunology Branch, NCI, and the [‖]NIA, National Institutes of Health, Bethesda, Maryland 20892, and the [¶]MOE Key Laboratory of Model Animal for Disease Study and Model Animal Research Center, Nanjing University, Nanjing 210061, China

Wnt signaling plays a key role in embryogenesis and cancer development. Dvl (Dishevelled) is a central mediator for both the canonical and noncanonical Wnt pathways. Dact1 (Dapper1, Dpr1), a Dvl interactor, has been shown to negatively modulate Wnt signaling by promoting lysosomal degradation of Dvl. Here we report that Dact1-deficient mice have multiple physiological defects that resemble the human neonate disease congenital caudal regression syndrome, including caudal vertebrae agenesis, anorectal malformation, renal agenesis/dysplasia, fused kidneys, and loss of bladder. These urogenital defects can be traced to impaired hindgut formation starting at embryonic day 8.25. Examination of morphological changes and Wnt target gene expression revealed that the planar cell polarity (PCP) signaling is deregulated, whereas the canonical Wnt/β-catenin pathway is largely unaffected in mutant embryos. Consistently, the activity of the PCP signal mediators Rho GTPase and c-Jun N-terminal kinase is altered in *Dact1*$^{-/-}$ mouse embryonic fibroblasts. We further observed alterations in the protein level and the cellular distribution of Dvl in the primitive streak of mutant embryos. An increased amount of Dvl2 tends to be accumulated in the cortical regions of the cells, especially at the primitive streak ectoderm close to the posterior endoderm that lately forms the hindgut diverticulum. Together, these data suggest that Dact1 may regulate vertebrate PCP by controlling the level and the cellular localization of Dvl protein.

Wnt signaling is crucial to determine the fates of cells during embryogenesis and for tissue homeostasis after birth. The alteration of Wnt signaling results in human congenital diseases and carcinogenesis (1–3). Wnt signaling is instigated by binding of extracellular Wnt ligands to Fz (Frizzled) transmembrane receptors, leading to membrane recruitment and activation of Dvl. From Dvl, Wnt signals diverge into at least two branches: the β-catenin-dependent canonical pathway and the β-catenin-independent noncanonical pathway. The canonical Wnt signaling promotes the disassembly of the β-catenin degradation complex of Axin, adenomatous polyposis coli, glycogen synthase kinase 3β, and casein kinase 1, the nuclear accumulation of β-catenin, and eventually β-catenin/T cell factor-mediated transcription. However, the noncanonical signaling such as planar cell polarity (PCP)[3] signaling is involved in cytoskeleton remodeling and influences cell polarity and movements via c-Jun N-terminal kinase (JNK), Rac GTPase, and Rho GTPase (4–7).

Mice with mutations in both the canonical and noncanonical Wnt pathways have been generated. Majority mice with mutations in canonical pathway components, such as low density lipoprotein receptor-related protein 6, Axin, and T cell factor 3, showed the defective phenotypes related to body axis (8–10), similar to Wnt3a knock-outs with paraxial mesoderm defects and loss of caudal somites (11–14). However, mutations in PCP components lead to the defects involved in cell polarity and convergent extension movements, which produce an elongation and narrowing of the tissue along the anterior-posterior axis (15–19). Given that Dvl functions at the cross-point of the canonical and noncanonical Wnt pathways, it would be expected that the Dvl knock-out mice showed the defective phenotypes overlapping with those in mutant mice of the canonical and noncanonical Wnt pathways. However, the phenotypes observed in Dvl-deficient mice are more reminiscent of PCP pathway defects, involving cochlea stereocilia orientation, neural tube closure, and also cardiac outflow tract development (20–24).

Dact (Dapper, Dpr), first identified as an interacting protein of Dvl, controls *Xenopus* embryogenesis by functioning as a general antagonist of Dvl to modulate the canonical and noncanonical Wnt signaling (25). Three Dact family members, including Dact1, Dact2, and Dact3, have been identified in zebrafish, mouse, and human (26–30). Recent studies suggested that the three Dact members may have distinct functions. In addition to the negative effect on Wnt signaling (25, 29, 31), Dact1 has been shown to enhance Wnt/β-catenin activity

* This work was supported, in whole or in part, by a National Institutes of Health Intramural Research Program grant (to Y. J. C.). This work was also supported by National Natural Science Foundation of China Grants 30930050 and 30921004 and 973 Program Grant 2006CB943401 (to Y.-G. C.).

[1] Both authors contributed equally to this work.

[2] To whom correspondence should be addressed. Tel.: 86-10-62795184; Fax: 86-10-62794376; E-mail: ygchen@tsinghua.edu.cn.

[3] The abbreviations used are: PCP, planar cell polarity; JNK, c-Jun N-terminal kinase; MEF, mouse embryonic fibroblast; E*n*, embryonic day *n*; GFP, green fluorescent protein; CMV, cytomegalovirus; RT, reverse transcription; ES cell, embryonic stem cell.

in zebrafish (28), similar to the function of Dact1 homolog Frodo in *Xenopus* (32). Our studies demonstrated that zebrafish and mouse Dact2 inhibit transforming growth factor-β/Nodal signaling during mesoderm induction by promoting lysosomal degradation of transforming growth factor-β type I receptors (27, 33). Zebrafish Dact2 may be also involved in the Wnt/PCP pathway because it is required for normal convergence extension movements in embryos (28). Human Dact3 has been shown to act as a negative regulator of Wnt/β-catenin signaling and may be associated with colorectal cancer formation (34). Consistent with the role of Dact3 in tumorigenesis, human Dact1 is down-regulated in hepatocellular carcinoma, and this down-regulation was correlated with the cytoplasm accumulation of β-catenin (35).

In the present study, we generated Dact1-deficient (*Dact1*$^{-/-}$) mice. Embryonic analyses revealed severe posterior malformations resulting from impaired hindgut development at E8–8.5. Furthermore, we found that PCP signaling was disrupted, whereas the canonical Wnt signaling remains largely normal in this region of *Dact1*$^{-/-}$ mice. The inactivation of Dact1 resulted in the enhanced expression and altered cellular distribution of Dvl2 in the malformed ectoderm of the primitive streak region. Consistent with the above findings, Dvl protein levels were also increased in *Dact1*$^{-/-}$ mouse embryonic fibroblasts (MEFs) in compared with wild-type cells. Our findings suggested that the dysfunctions of PCP signaling mediated by the elevated activity of Dvl might account for the posterior malformations in *Dact1*$^{-/-}$ mice.

EXPERIMENTAL PROCEDURES

Generation of Dact1$^{-/-}$ *Mice*—All of the mice used in this study were bred and maintained on a normal 12-h light/12-h dark cycle and provided regular mouse chow and water *ad libitum* in an Association for Assessment and Accreditation of Laboratory Animal Care-accredited specific pathogen-free facility (Model Animal Research Center, Nanjing University). A 3.5-kb sequence containing 3′ sequence of the *Dact1* gene was amplified by PCR from a 129/Sv mouse genomic library using two primers (5′-CTCGAGGATATCTGGTTTGTGCAATAGCTC-3′ and 5′-GCGGCCGCGATGGTTATACCGAGACC-3′), which contain XhoI/EcoRV and NotI restriction sites, respectively. The amplified fragment was inserted into the XhoI-NotI sites of the vector ploxP (36) to generate ploxP-*Dact1*-3′arm. A 3.5-kb 5′ homologous arm was obtained by PCR with two primers (5′-ATCGATAAGGTGTGTTCTAGAGGACTC-3′ and 5′-GTCGACAAACAAGCAAGGACGTTG-3′) containing ClaI and SalI, respectively, and then inserted into the corresponding sites of the recombinant plasmid ploxP-*Dact1*-3′arm to generate the *Dact1* targeting vector. Electroporation of embryonic stem (ES) cells and generation of germ line chimeras were done with standard procedures (37). Gene targeting was confirmed by Southern blot with EcoRV-digested genomic DNAs from ES cells or animal tails. A 2.1-kb sequence corresponding to the *Dact1* 3′-flanking genomic fragment was amplified using primers (5′-CATGATATTGCAAGTATGG-3′ and 5′-ACTGAATAATGTAAGGGAAC-3′) from the 129/Sv mouse genomic library and inserted into pGEM-T easy vector (Promega) to generate the probe construct. The Southern probe was prepared by digesting the plasmid with HpaI and EcoRV and detected a 16-kb fragment from the wild-type allele as well as a 5.5-kb fragment from the targeted allele (see Fig. 1).

Genotypic Analysis—The mice were genotyped by Southern blot as described above or by PCR. For PCR analysis, the primers GDAP1F1 (5′-TAAACGGAGGCACAAGGAGG-3′) and GDAP1R1 (5′-AAGCTAATGTCCACTCGGTAC-3′) from the *Dact1* genomic sequence amplified a 400-bp fragment from the wild-type allele (see Fig. 1). The combinatory use of primer GDAP1F1 and primer Neo1 (5′-TTCTGGATTCATCGACTGTG-3′) amplified a 1-kb fragment from the mutant allele.

Histology and Immunohistochemistry—Tissues were dissected and fixed in 4% paraformaldehyde at 4 °C overnight, dehydrated, embedded in paraffin, sectioned at 8 μm, and stained with hematoxylin and eosin. Photographs were taken using an Olympus light microscope with a digital camera. Immunofluorescence assays were performed on frozen sections. α-Dvl2 was from Cell Signaling, and rhodamine phalloidin was from Invitrogen. E8–8.5 embryo transverse sections (15 μm) were examined under a Zeiss LSM 710 laser scanning microscope at identical illumination conditions and further processed with ZEN 2009 Software (Carl Zeiss). Integral optical density of the ectoderm area was measured using Image-Pro Plus 6.0 software (Media Cybernetics), and equal-sized squares along the ectoderm were measured in wild-type or *Dact1*$^{-/-}$ embryos.

Skeletal Staining and Whole Mount in Situ Hybridization—Skeletal staining with Alcian Blue and Alizarin Red and whole mount *in situ* hybridization were performed as described (38, 39). The *Dact1 in situ* probe corresponding to its coding sequence (1250–1601 nucleotides) was cloned as described (30). The *Axin2* probe was kindly provided by Drs. F. Costantini and E.-H. Jho (40), and the probes of *Shh* (*sonic hedgehog*), *Pax1* (*paired box gene 1*), and *Pax3* (*paired box gene 3*) were described (41).

Cell Culture and Lentiviral Constructs—All of the cell lines were maintained in Dulbecco's modified essential medium supplemented with 1% penicillin-streptomycin, 10% fetal calf serum at 37 °C in a humidified, 5% CO_2 incubator. Mouse Wnt3a-conditioned medium was produced as previously described (31). Primary MEFs were isolated and cultured as previously described (39). The Dact1 overexpression in MEFs was reintroduced by a lentiviral system, using GFP as control. pHR′-CMV-GFP lentiviral constructs were described previously (42). The Dact1 cDNA was inserted to the BamHI-XhoI sites of pHR′-CMV-GFP to replace the GFP fragment. The vesicular stomatitis virus glycoprotein pseudotyped lentiviral vector was generated by transient cotransfection of the vector construct pHR′-CMV-GFP or pHR′-CMV-Dact1 (12 μg) with the vesicular stomatitis virus glycoprotein-expressing construct pMD.G (6 μg) and the packaging construct pCMV-ΔR8.9 (9 μg) into 293T cells. The medium was replaced with fresh medium at 12 h after transfection. Then the lentivirus was harvested at 36 and 60 h after transfection. The cells were harvested at 72 h after lentiviral infection.

Glutathione S-Transferase-Rho-binding Domain Binding Assay and Immunoblotting—Glutathione *S*-transferase-Rho-binding domain binding assay for detection of GTP binding activity of RhoA was performed as described (43). For immunoblotting, the cells in 100% confluency were lysed at 4 °C for 10 min with lysis solution (50 mM Tris, pH 7.5, 150 mM NaCl, 1 mM

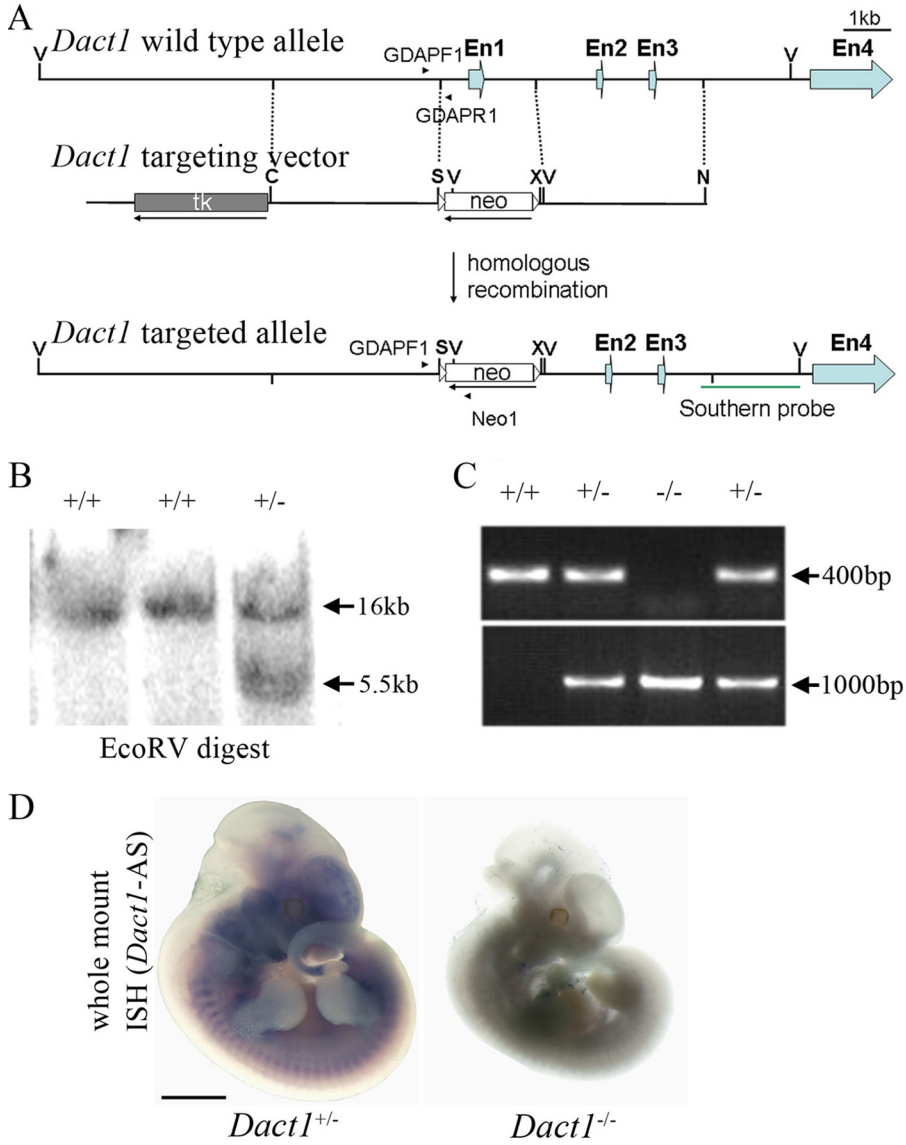

FIGURE 1. **Targeted inactivation of the *Dact1* gene.** *A*, diagrams of the wild-type *Dact1* allele (*top*), the construct used for generating the targeted allele (*middle*), and the inactivated gene after homologous recombination (*bottom*). A PGKneo cassette was inserted in the opposite orientation relative to *Dact1* transcription, and the promoter region, exon 1, and partial intron 1 were deleted to generate *Dact1* null. *En*, Exon; *V*, EcoRV; *S*, SalI; *X*, XhoI; *N*, NotI. *GDAPF1*, *GDAPR1*, and *NEO1* stand for genotyping primers. *B*, genomic DNA Southern blot analysis of ES cells. Using the 3′-flanking probe indicated in Fig. 1*A*, a 5.5-kb EcoRV fragment appears in the targeted clone in addition to the 16-kb EcoRV wild-type fragment. *C*, PCR genotyping of genomic tail DNA. Using the PCR primer pairs indicated in *A*, wild-type and knock-out loci generate 400- and 1000-bp fragments, respectively. *D*, whole mount *in situ* hybridization shows the absence of *Dact1* transcripts in *Dact1*$^{-/-}$ embryos. *Scale bar*, 5 mm.

EDTA, 0.5% Nonidet P-40, 10 mM NaF, 20 mM sodium β-glycerol phosphate, 1 mM dithiothreitol, and protease inhibitors), and the lysates were analyzed by SDS-PAGE, immunoblotted with various antibodies, and detected with a enhanced chemiluminescent substrate (Pierce). The antibodies used were as follows: α-Dvl2 (Cell Signaling), α-activated β-catenin (Millipore), α-β-catenin (Zymed Laboratories Inc.), α-β-actin (Sigma), α-Dvl3 (kindly provided by Dr. Lin Li), α-Dpr1 (described in Ref. 29). Other antibodies were from Santa Cruz Biotechnology.

Luciferase Assays—MEFs were seeded in 24-well dishes in a primary density of 8×10^4 cells/well for 18 h prior to transfection. Transfection was performed with Lipofectamine 2000 (Invitrogen). Luciferase activity was measured at 48 h after transfection using a dual-luciferase reporter assay system (Promega). Reporter activity was normalized to cotransfected *Renilla*. The experiments were repeated in triplicate.

Real Time RT-PCR—Real time RT-PCR was performed using total RNA isolated from MEFs and repeated at least three times for each gene with Stratagene MX3000PTM system using a SYBR Green assay. The expression values were normalized to *GAPDH* expression. The primer sequences are as follows: *Axin2*, 5′-GCAGCAGATCCGGGAGGATGAA-3′, and 5′-GATTGACAGCCGGGGGTCTTGA-3′; c-*myc*, 5′-TGAGCCCCTAGTGCTGCAT-3′ and 5′-AGCCCGACTCCGACCTCTT-3′; *GAPDH*, 5′-CATGGCCTTCCGTGTTCCTA-3′ and 5′-CCTGCTTCACCACCTTCTTGAT-3′.

RESULTS

Generation of Dact1-deficient Mice—We generated constitutive *Dact1* knock-out mice by conventional knock-out approaches using 129/SV ES cells. A 2-kb fragment including a part of the promoter region, entire exon 1 containing the translation initiation code ATG and partial intron 1 was replaced by a reversed neomycin resistance cassette (Fig. 1*A*). Southern blot (Fig. 1*B*) and genotyping PCR (Fig. 1*C*) were employed to identify the targeted allele in ES cells, mice, and embryos. The absence of *Dact1* transcripts in *Dact1*$^{-/-}$ embryos was verified by whole mount *in situ* hybridization (Fig. 1*D*) and RT-PCR (not shown).

Majority of Dact1$^{-/-}$ *Neonates Were Born Runt and Perinatally Lethal*—*Dact1*$^{+/-}$ mice were first bred in a mixed B6;129/SV background and then backcrossed for more than five generations to C57BL/6 background before use in this study. Strikingly, there were 25 *Dact1*$^{+/+}$, 50 *Dact1*$^{+/-}$, and only one *Dact1*$^{-/-}$ in 76 adult mice from F2 *Dact1*$^{+/-}$ intercrosses, which was dramatically distinctive from the expected Mendelian segregation, suggesting that *Dact1*$^{-/-}$ mouse died either at embryonic stages or before weaning. Indeed, isolation of E18.5 embryos showed that the ratio (12:24:12) of *Dact1*$^{+/+}$, *Dact1*$^{+/-}$, and *Dact1*$^{-/-}$ embryos from *Dact1*$^{+/-}$ mouse intercrosses was equivalent to the expected Mendelian segregation, indicating

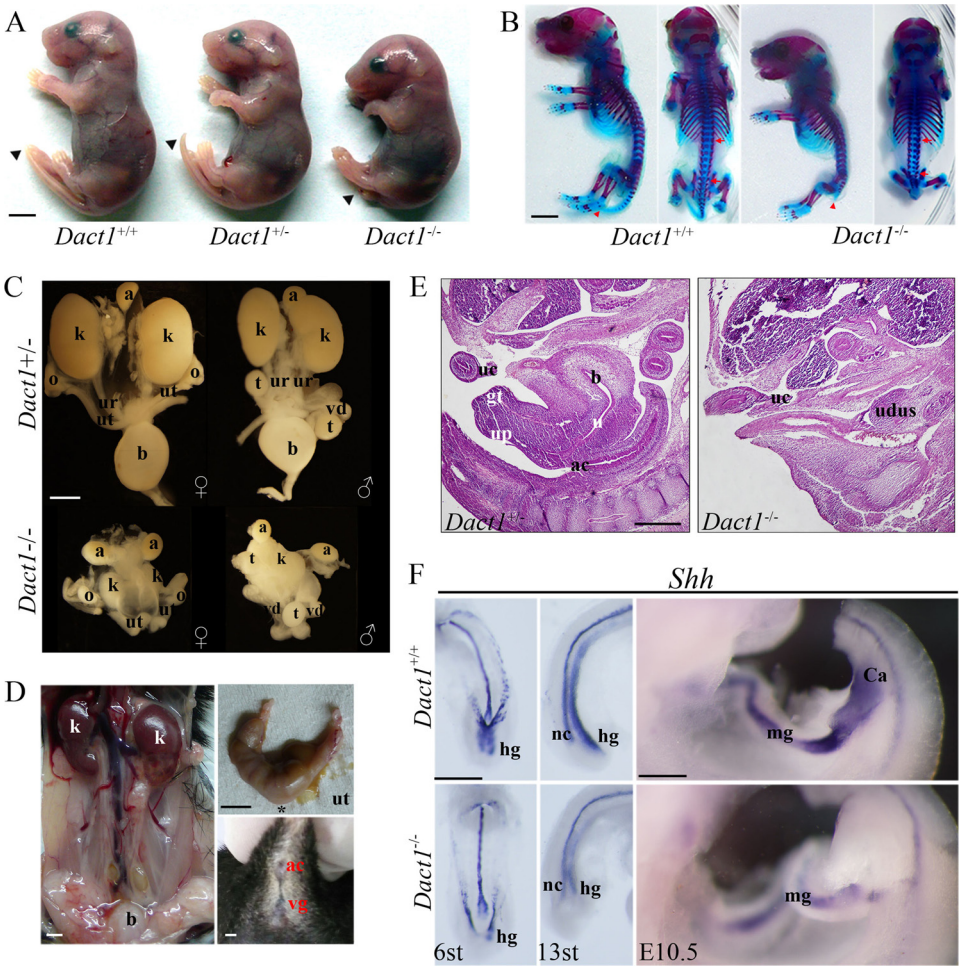

FIGURE 2. **Dact1$^{-/-}$ mice are perinatal lethal with posterior malformation associated with severe urogenital defects.** *A*, *Dact1*$^{-/-}$ mutants are born runt, with a short body and a short tail (*arrowhead*), compared with its wild-type and heterozygous siblings. *B*, double staining of newborn skeletons. E18.5 embryos were stained with Alizarin Red (bone) and Alcian Blue (cartilage). Most of the skeletons are the same between wild type and mutants, except for the caudal vertebrae (*red arrowheads*). The mutant exhibited malformed sacral vertebrae and condensed lumbar vertebrae (the region between the *red arrows*). More than four embryos were examined. *C*, the urogenital system outline of E17.5 embryos. The mutant (*lower panels*) showed abnormal fused hydronephrotic kidneys (*k*), lack of bladder (*b*), unidentified ureters (*ur*), misconnected blind-ended uteruses (female, *ut*) or van deferens (male, *vd*), compared with the heterozygous siblings (*upper panels*). In contrast, the adrenal glands (*a*), ovaries (*o*), and testes (*t*) of mutant embryos were in normal size and right position. *D*, phenotypes of *Dact1*$^{-/-}$ surviving female adult. The mutant 10-month-old female had mild cystic kidneys (*k*), lack of vagina (*) (*left panel*), and uterine (*ut*) hydrometra (*upper right panel*). The *lower right panel* showed no vagina open (*vg*) adjacent to the anal canal (*ac*). *E*, hematoxylin- and eosin-stained mid-sagittal section of E13.5 *Dact1*$^{+/-}$ (*left panel*) and *Dact1*$^{-/-}$ (*right panel*) specimens. The mutant showed a mass of undifferentiated urogenital tissues, instead of developing urogenital tract seen in its heterozygous sibling. *ac*, anal canal; *b*, bladder; *gt*, genital tubercle; *uc*, umbilical cord; *up*, urethral plate; *udus*, undifferentiated urogenital tissues. More than four embryos were examined. *F*, *Shh* expression in developing caudal region of wild-type (*upper panel*) and *Dact1*$^{-/-}$ (*lower panel*) embryos at E8.25 (6 somites) (*left panel*, ventral view), E9 (13 somites) (*middle panel*, lateral view), and E10.5 (*right panel*, lateral view), as shown by whole mount *in situ* hybridization. *Shh* mainly expressed in notochord (*nc*), and gut epithelia, including midgut (*mg*) and hindgut (*hg*). The mutant showed truncated and no dilated hindgut and shorter notochord (*left* and *middle panels*). At E10.5, no cloaca (*Ca*) swelled in mutant embryos. More than five mutant embryos have been employed for each stage. *st*, somites; *scale bar*, 5 mm in *A*, *B*, and *D*, and 0.5 mm in *C*, *E*, and *F*.

that the death of most of *Dact1*$^{-/-}$ mice occurred perinatally. The only surviving female adult of *Dact1*$^{-/-}$ was viable but infertile.

To understand what caused the death of *Dact1*$^{-/-}$ mice, newborn pups were examined. *Dact1*$^{-/-}$ pups were born with a short body and a short tail (Fig. 2*A*), compared with *Dact1*$^{+/+}$ and *Dact1*$^{+/-}$ siblings, indicating caudal developmental defects as observed in Wnt3a, Wnt5a, low density lipoprotein receptor-related protein 6, and Ltap-deficient mice (9, 13, 44, 45). Scrutiny of litters at birth showed that newborn *Dact1*$^{-/-}$ pups died within 24 h. To investigate the short and somewhat curly body of *Dact1*$^{-/-}$ embryos, we examined bone and cartilage development using Alizarin Red and Alcian Blue staining at E18.5. Major defects were localized caudally in the coccyges (Fig. 2*B*). Consistent to the observation of the loss of most caudal coccyges, we also found the caudal lumbar vertebrae and the ilia were often malformed. However, the sacral vertebrae remained intact. Total lumbar numbers of *Dact1*$^{-/-}$ embryos were equivalent to that of wild type, but the intervals between lumbar vertebrae were slightly decreased in *Dact1*$^{-/-}$ (Fig. 2*B*), implying mild defects of somitogenesis and segmentation at late stages in the last few somites. The numbers and shapes of thoracic vertebrae, ribs, and limbs were grossly normal.

Dact1$^{-/-}$ *Lethality Is Due to Urogenital Defects*—In addition to short tails in *Dact1*$^{-/-}$ neonates, the external genitalia and anuses, as well as the outlet of urethrae, were absent (15 of 15) (Fig. 2*E*). The severity of these defects could contribute to the perinatal lethality of *Dact1*$^{-/-}$ newborn pups (44). Inside, *Dact1*$^{-}$/$^{-}$ embryos exhibited severe defects on kidneys and the urogenital tracts (Fig. 2*C*). Renal malformations were observed from E12.5 to postnatal day 0. 84% of *Dact1*$^{-/-}$ embryos showed mid-fusion (16 of 19), 11% showed unilateral agenesis (2 of 19), and 5% had no kidney (1 of 19) under the most severe circumstances. 11 of 12 *Dact1*$^{-/-}$ embryos at E17.0 or later stages showed typical hydronephrosis, whereas the one without hydronephrotic symptoms had one kidney and entire ureter-bladder tract. 18 of 19 *Dact1*$^{-/-}$ embryos mentioned above had no bladders. The mutant ureters were blind-ended, usually too thin or too short to be identified. The female uteruses or male van deferens were blind-ended with erroneous connection. In contrast, the adrenal glands, ovaries, and testes in *Dact1*$^{-/-}$ embryos were grossly normal. In addition, the rare surviving female adult of *Dact1*$^{-/-}$ also had defects in genital urinary system. Fig. 2*D* showed mild cystic kidneys, uterine hydrometra, and lack of vagina in the surviving *Dact1*$^{-/-}$ adult female, consistent with infertility of the surviving mutant.

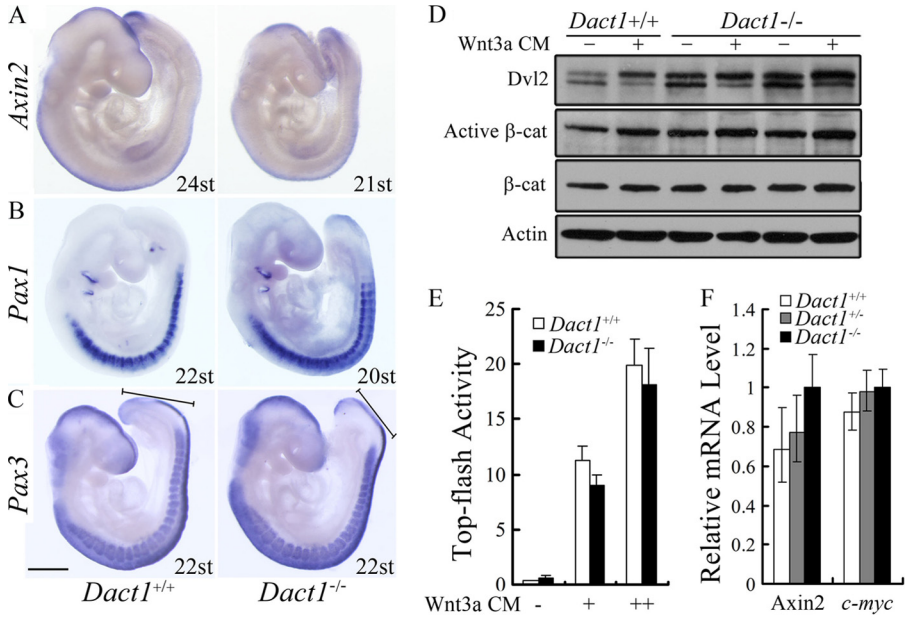

FIGURE 3. **The canonical Wnt signaling is largely normal in *Dact1*$^{-/-}$ mice.** *A*, wild-type (*left*) and *Dact1*$^{-/-}$ (*right*) embryos showed no difference in Axin2 expression using whole mount *in situ* hybridizations of E9.5 littermates. *st*, somites. *B* and *C*, paraxial mesoderm was intact in *Dact1*$^{-/-}$ embryos. The expression of the somatic markers *Pax1* (*B*) and *Pax3* (*C*) confirmed the presence of paraxial mesoderm throughout the axis of *Dact1*$^{-/-}$ embryos. *Black lines* with *blunt ends* (**C**) show the length of presomitic mesoderm, which was shorter in *Dact1*$^{-/-}$ than in *Dact1*$^{+/+}$ embryos. More than five mutant embryos have been employed for each probe. *st*, somites; *scale bar*, 0.5 mm. *D*, the Dvl2 protein level is increased in *Dact1*$^{-/-}$ MEFs. Three lines of *Dact1*$^{+/+}$ or *Dact1*$^{-/-}$ MEFs were treated with Wnt3a conditioned medium (*Wnt3a CM*) or control medium for 8 h, and the cell lysates were subjected to immunoblotting with the indicated antibodies. The β-actin was used as a loading control. A slight increase of active β-catenin level was also seen in *Dact1*$^{-/-}$ cells. *E*, MEF cells seeding in 24-well plate were transfected with Top-flash (1 μg) and *Renilla* (50 ng) and then harvested at 48 h post-transfection for luciferase assay. The cells were treated with control medium or Wnt3a CM at a dilution of 1:10 or 1:5 for 12 h before harvest. *F*, expression of *Axin2* and c-*myc* in *Dact1*$^{+/+}$, *Dact1*$^{+/-}$, or *Dact1*$^{-/-}$ MEF cells were measured by real time RT-PCR. For luciferase assay and real time RT-PCR, each experiment was performed in triplicate, and the data represent the means ± S.D. after normalized to *Renilla* activity or the *GAPDH* expression level.

No Cloaca Is Formed at the Early Developmental Stages of Dact1$^{-/-}$ *Embryos*—After defining the urogenital defects in *Dact1*$^{-/-}$ embryo at E18.5, we decided to trace back to the earlier stages when the defects emerged in mutant embryos. First it was confirmed that there were no developing genital tubercles and the total sets of bladder, urethra, and anal canal in *Dact1*$^{-/-}$ embryos at E13.5 (Fig. 2*E*). This excluded the possibility of genital tubercle dysplasia, as shown in *Shh* mutant embryos (46). We then observed the morphologic changes in the urigenital sinus at E11.5 (data not shown), the cloaca at E10.5, and the hindgut at E8.25-E9.5, using *Shh* as the epithelium marker (Fig. 2*F*). As expected, at E10.5, *Dact1*$^{-/-}$ embryos had no cloaca, and the midgut extension stopped at the presumptive position of cloaca. Consistently, at E8.25 (6 somites), the posterior endoderm of *Dact1*$^{-/-}$ embryos did not extend caudally as far as that of wild-type embryos and failed to fold ventrally, leading to formation of a disorganized hindgut diverticulum. At E9 (13 somites), evident posterior malformation in the presomitic mesoderm region appeared in the null embryos. Other morphological abnormalities in *Dact1*$^{-/-}$ embryos included truncated, twisted notochord, and no dilated hindgut, compared with wild-type siblings. Another finding was that the *Shh* level decreased in the gut regions of the mutants, indicating a decrease of the gut epithelium structure in *Dact1*$^{-/-}$ embryos. The studies for earlier stages (from E8.25 to E13.5) of *Dact1*$^{-/-}$ embryos indicated that Dact1 protein is necessary and essential in embryogenesis initiating at E8.25, at least.

The Canonical Wnt Signaling Is Largely Unaffected in Dact1$^{-/-}$ *Embryos*—To understand the molecular basis accounting for defects in the hindgut of *Dact1*$^{-/-}$ embryos, we examined whether the canonical Wnt signaling is altered. *Axin2* is a well defined target of the canonical Wnt signaling, mainly expressed along the neural tubes and the presomitic mesoderm. Whole mount *in situ* hybridization analysis revealed there was no difference in *Axin2* expression between *Dact1*$^{+/+}$ and *Dact1*$^{-/-}$ embryos. The slight decrease in the tail buds of mutants was due to the severely malformed structures (Fig. 3*A*). Most of the null mutants of canonical Wnt pathway components have primary defects resulting from the formation of ectopic neural tissue at the expense of paraxial mesoderm (13, 14, 47, 48). To follow the fate of paraxial mesoderm, we examined two somitic markers, *Pax1* and *Pax3*. The sclerotome marker *Pax1* revealed that somites were present (Fig. 3*B*). Similarly, detection of *Pax3* transcripts, normally present in dermomyotome, migrating muscle progenitor cells, and developing sclerotome compartments, clearly distinguished the presence of somitic tissue along the entire anterior-posterior axis of *Dact1*$^{-/-}$ embryos (Fig. 3*C*). Although *Dact1*$^{-/-}$ embryos appeared disorganized at the caudal end, as indicated by the length of the presomitic mesoderm, no somites were affected at this stage. These results suggested that paraxial mesoderm fate is unaffected in *Dact1*$^{-/-}$ embryos.

To further confirm that there was no obvious anomaly for the canonical Wnt/β-catenin signaling in *Dact1*$^{-/-}$ embryos, we isolated MEFs and determined the active β-catenin level (Fig. 3*D*), the Topflash reporter activity (Fig. 3*E*), and the expression level of target genes *Axin2* and c-*myc* in these cells (Fig. 3*F*). The canonical Wnt signaling showed no significant differences in *Dact1*$^{-/-}$ MEFs in comparison with wild-type cells. However, the increased level of Dvl2 protein was clearly noticed in *Dact1*$^{-/-}$ MEFs (Fig. 3*D*), whereas the Dvl2 mRNA level was not evidently changed in *Dact1*$^{-/-}$ MEFs (data not shown), consistent with previous reports that Dact1 destabilizes Dvl proteins (29).

The PCP Signaling Is Deregulated in Dact1$^{-/-}$ *Embryos*—Because Dact1 is a negative regulator of both canonical and noncanonical Wnt signaling (25, 29), we speculated that PCP signaling might be altered in *Dact1*$^{-/-}$ mutants. Indeed, the

neural tube in *Dact1*$^{-/-}$ embryos was significantly broader than in wild-type siblings (Fig. 4*A*), suggesting defects in neural tube elongation. In agreement with this, we observed significantly broadened neural tubes in E9.5 *Dact1*$^{-/-}$ embryo tail buds (Fig. 4*B*), indicating that *Dact1* plays a role in neural plate convergent extension and neural tube closure (21). These data together suggest that PCP signaling was deregulated in the absence of Dact1, which was further supported by the data that RhoA GTPase and JNK activities, markers of PCP signaling, were changed with less active RhoA but more active JNK in *Dact1*$^{-/-}$ MEFs (Fig. 4, *C* and *D*). Consistent with the increased level of Dvl2 in *Dact1*$^{-/-}$ MEFs, Dvl3 was also increased (Dvl1 was undetectable in MEFs) (Fig. 4*D*). The effect of Dact1 on PCP signaling was further confirmed by reintroduction of Dact1 into *Dact1*$^{-/-}$ MEFs, and Dact1 expression restored Dvl2/3, p-JNK, and active RhoA levels in *Dact1*$^{-/-}$ MEFs similar to the ones in wild-type cells (Fig. 4, *C* and *D*).

Then we investigated whether there are any alterations in the level and distribution of Dvl2 protein in the hindgut region, where the morphologic abnormalities occurred at E8.25 *Dact1*$^{-/-}$ embryos (Fig. 4*E*; note the malformed endoderm). Immunofluorescence staining revealed an increased expression of Dvl2 protein in the primitive streak area, where hindgut starts to form, in *Dact1*$^{-/-}$ embryos, especially in the ectoderm region (Fig. 4, *E* and *F*). Interestingly, remarkable intensified staining of Dvl2 was also observed in the cortical regions of the ectodermal cells in *Dact1*$^{-/-}$ embryos, whereas the intensity tended to evenly distribute in the corresponding region of wild type (Fig. 4*E*). The disrupted cell polarity, signed by phalloidin-stained F-actin, was also observed in the ectoderm of *Dact1*$^{-/-}$ embryos at E8.5 (7–8 somites) (Fig. 4*G*), albeit not in E8.25 (5 somites) (Fig. 4*E*). Together, these data suggest that the altered Dvl protein level and distribution by inactivation of Dact1 may lead to deregulation of PCP signaling in the primitive streak, which contributes to the posterior malformation in *Dact1*$^{-/-}$ embryos.

DISCUSSION

Dact1 functions as a negative regulator of Wnt signaling by promoting Dvl degradation. In this study, we showed that inactivation of the Dact1 gene leads to posterior malformation and perinatal lethality of mice. The urogenital defects are due to impaired hindgut formation in the primitive streak at E8.25. Further analyses revealed that the PCP signaling, but not the canonical Wnt signaling, is deregulated, which most likely results from the altered protein level and distribution of Dvl2 in the ectoderm region of the primitive streak.

The phenotypes of Dact1 null mice resemble the human neonate disease congenital caudal regression syndrome, and the defective phenotypes include caudal vertebrae agenesis, anorectal malformation, renal agenesis/dysplasia, fused kidneys, as well as bladder loss (49–51). However, only a small percentage of *Dact1*$^{-/-}$ embryos mimic the sacral agenesis symptom of congenital caudal regression syndrome, suggesting a more specified syndrome spectrum in *Dact1*$^{-/-}$ embryos. Developmental defects of kidneys in *Dact1*$^{-/-}$ mice could be traced back to E11.5 when the ureteric bud branches into metanephric mesenchyme and begins to generate the definitive renal collecting system and to induce formation of renal vesicles (52, 53). Despite the loss of cloaca, the Wolffian duct elongates and the ureteric bud develops normally in *Dact1*$^{-/-}$ embryos. However, the two metanephric rudiments derived from the ureteric bud are much closer to each other than in wild type. Furthermore, no *Dact1* mRNA expression was detected in the metanephros. This suggested that the severe kidney abnormalities may occur secondarily, which can be partly attributed to the small volume of the caudal parts.

Dact1$^{-/-}$ embryos display an intact paraxial mesoderm, an abnormally closed posterior neuroectoderm, but a twisted notochord and a significantly impaired caudal endoderm, but *Dact1* mRNA is mainly expressed in the posterior ectoderm and mesoderm (30) (data not shown). Therefore, the abnormal phenotypes are not well correlated with *Dact1* mRNA expression. This may be due to the discordant protein and mRNA expression patterns (54). Unfortunately, the lack of specific antibodies against Dact1 protein prohibits us from examining Dact1 protein expression. Another possibility is that the cells in the posterior ectoderm and mesoderm may produce signals that are required for proper development of not only the neuroectoderm and notochord but also the adjacent endoderm. Posterior endoderm started to become malformed at the site where notochord is adjacent to the gut, indicating that the molecular changes in notochord possibly influence hindgut formation, as previously reported (55).

Our findings suggested that the phenotypes observed in *Dact1*$^{-/-}$ embryos result from the altered expression and distribution of Dvl protein. Previous work has linked the abnormalities in cardiac outflow tract, cochlea, and neural tube closure in Dvl knock-outs to impaired PCP signaling (24). The defective neural tube closure and posterior malformation were also observed in *Dact1*$^{-/-}$ embryos, indicating that PCP signaling was disrupted by *Dact1* inactivation. Both gain-of-function and loss-of-function of Dsh/Dvl have been reported to result in convergent extension movement defect in *Xenopus* embryos (56–59). We have also observed altered Dvl2 distribution in the cortical regions of the cells in the *Dact1*$^{-/-}$ E8.25 primitive streak ectoderm. The subcellular distribution of Dvl may be directly associated to its physiological functions in regulating PCP. It was reported that the DEP domain, which plays an essential role in Dsh/Dvl-mediated PCP signaling in *Drosophila* and *Xenopus* (21, 56–59), was required for Dvl2 to regulate neurulation in mouse embryos (23). Consistent with the role of Dact1 in PCP signaling, the alteration of RhoA and JNK activity was observed in *Dact1*$^{-/-}$ MEFs. The change of RhoA and JNK activities in opposing directions was reported in disrupted PCP signaling related to mouse neural tube closure (60, 61). However, the defects of *Dact1*$^{-/-}$ mice might also be due to other mechanisms because Dact1 has been reported to regulate Wnt signaling independent of the Dvl pathway (31, 62, 63).

During the preparation of this manuscript, Suriben *et al.* (64) reported a *Dact1*$^{-/-}$ mutant with a deletion of exon 2. The phenotypes of that mutant, including perinatal lethality, caudal regression, absent bladder, and the fused hydronephric kidneys, are very similar to those of our mutant. They also found that PCP signaling, but not canonical Wnt signaling, is responsible for the posterior malformation in hindgut. The difference

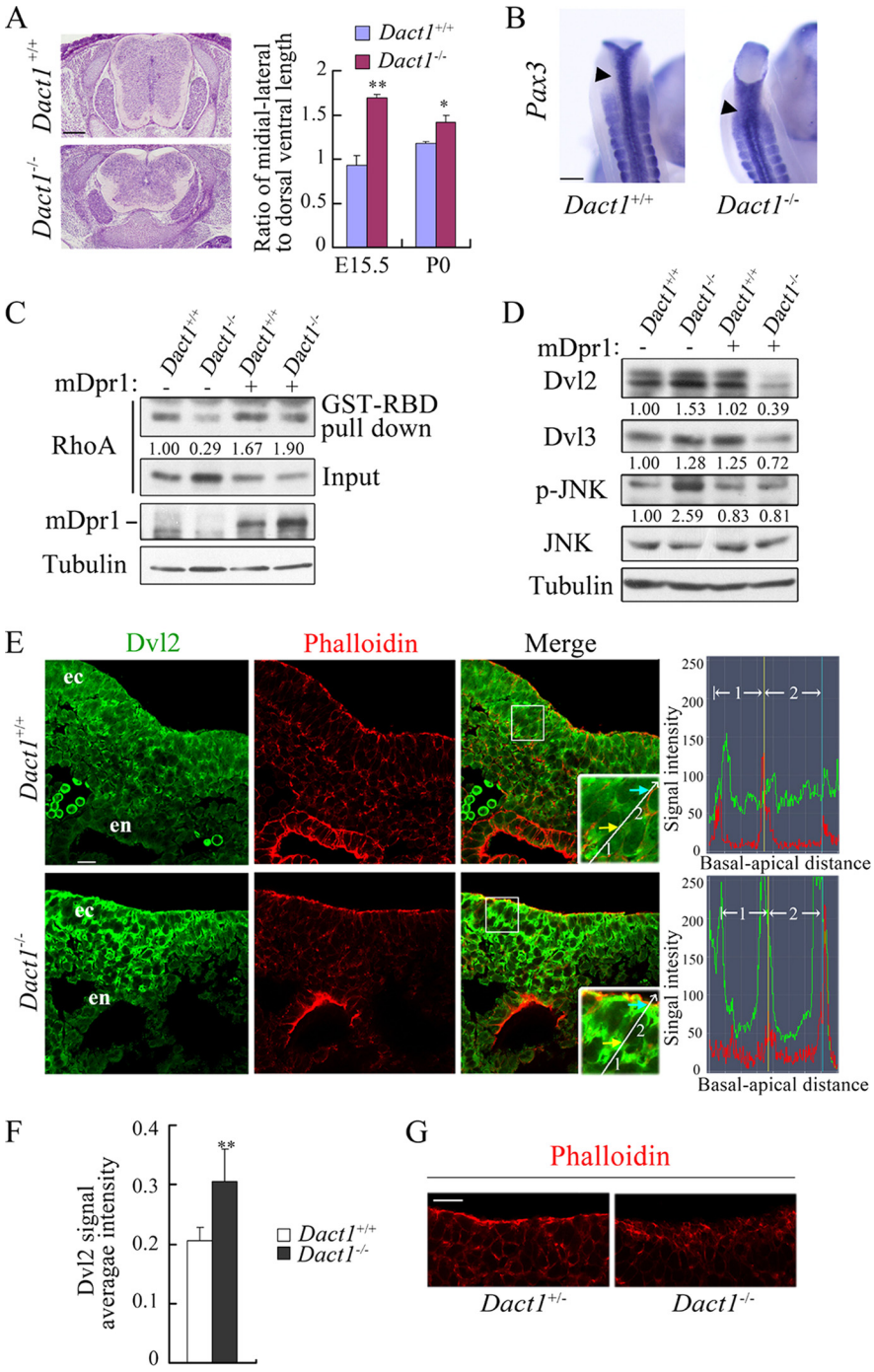

FIGURE 4. **Deregulation of the PCP signaling is associated with altered Dvl activities in Dact1$^{-/-}$ mice.** *A*, E15.5 wild-type and *Dact1*$^{-/-}$ embryos transversely sectioned through the lumbar. The neural tube was significantly wider in mutants than in wild-type siblings. At the E15.5 and postnatal day 0 stages, ratios of medial-lateral to dorsal-ventral axis were statistically analyzed in *Dact1*$^{+/+}$ and *Dact1*$^{-/-}$ mice, respectively. **, $p < 0.01$; *, $p < 0.05$. More than four embryos were examined. *B*, malformed neural tube closure (*arrowhead*) is shown in E9.5 *Dact1*$^{-/-}$ embryos in the last several somites by whole mount *in situ* hybridization staining of *Pax3* (dorsal view). *C*, decreased level of RhoA-GTP in *Dact1*$^{-/-}$ MEF as shown by pulldown assay. Glutathione *S*-transferase-Rho-binding domain, which specifically binds to RhoA-GTP (50 μg each), was added in equal cell lysates of *Dact1*$^{+/+}$ and *Dact1*$^{-/-}$ MEF with or without Dact1 overexpression. After incubation in 4 °C for 1 h, RhoA was examined by anti-RhoA immunoblotting. Inputs (10% of total lysates) are shown in the *lower panels*. The endogenous protein levels of Dact1 were not detected because of the limited antibody sensitivity. The band density was quantitated by BandScan software (Glyko), and the relative density of pulled down RhoA was normalized to the total RhoA (input) in the same sample. *D*, MEF lysates (the same batch of cells prepared as in *C*) were subjected to immunoblotting with the indicated antibodies, and tubulin was used as a loading control. The relative density of Dvl2/3 in each lane was normalized to tubulin in the same sample, and the relative density of p-JNK was normalized by total JNK. *E*, E8.25 (5 somites) embryos were transversely sectioned at the primitive streak region, and indirect anti-Dvl2 immunofluorescence (*green*) was performed. Phalloidin stains F-actin (*red*). The images were taken by a Zeiss LSM 710 laser scanning microscope under identical illumination conditions and processed with Zen2009 software. *Insets*, a higher magnification highlights Dvl2 distribution patterns in ectoderm cells. A *straight line* indicates the direction from basal to apical side of two adjacent cells (designated as *1* and *2* sequentially), and signal intensity of Dvl2 (*green*) or phalloidin (*red*) along the line was shown in the *right graphs*. The *yellow* and *blue arrows* point to the cell boundary, and they correspond to the points shown as lines of the same colors in the *right graphs*. *ec*, ectoderm; *en*, endoderm. *F*, integral optical density of nine equal-sized squares along the ectoderm was measured in wild-type or *Dact1*$^{-/-}$ embryos, respectively, with Image-Pro Plus 6.0 software. Dvl2 signal average intensity = (integral optical density sum)/area. **, $p < 0.01$. *G*, phalloidin staining of F-actin in the primitive streak region of E8.5 (7–8 somites) embryos. *Scale bars*, 20 μm in *E* and *G*; 0.5 mm in *A* and *B*.

between these works is the possible molecular mechanism underlying these defects. They reported that Dact1 is genetically interacted with a PCP component Vangl2, whereas our data showed that alteration of Dvl activity may account for Dact1 loss-induced defects. We found that the increase of Dvl2 protein expression was restricted in the ectoderm and adjacent mesoderm in the primitive streak regions. Nonetheless, these works together demonstrate an essential role for Dact1 in the modulation of posterior development in mouse embryos.

Acknowledgments—We thank Drs. Frank Costantini and Eek-hoon Jho for probes, Lin Li for antibodies, and Anming Meng, Qinghua Tao, Wei Wu, and Jian Zhang for fruitful discussion.

REFERENCES

1. Moon, R. T., Kohn, A. D., De Ferrari, G. V., and Kaykas, A. (2004) *Nat. Rev. Genet* **5,** 691–701
2. Clevers, H. (2006) *Cell* **127,** 469–480
3. Logan, C. Y., and Nusse, R. (2004) *Annu. Rev. Cell Dev. Biol.* **20,** 781–810
4. Angers, S., and Moon, R. T. (2009) *Nat. Rev. Mol. Cell Biol.* **10,** 468–477
5. Wang, J., and Wynshaw-Boris, A. (2004) *Curr. Opin. Genet. Dev.* **14,** 533–539
6. Huang, H., and He, X. (2008) *Curr. Opin. Cell Biol.* **20,** 119–125
7. Wu, D., and Pan, W. (2010) *Trends Biochem. Sci.*, in press
8. Zeng, L., Fagotto, F., Zhang, T., Hsu, W., Vasicek, T. J., Perry, W. L., 3rd, Lee, J. J., Tilghman, S. M., Gumbiner, B. M., and Costantini, F. (1997) *Cell* **90,** 181–192
9. Pinson, K. I., Brennan, J., Monkley, S., Avery, B. J., and Skarnes, W. C. (2000) *Nature* **407,** 535–538
10. Merrill, B. J., Pasolli, H. A., Polak, L., Rendl, M., García-García, M. J., Anderson, K. V., and Fuchs, E. (2004) *Development* **131,** 263–274
11. Liu, P., Wakamiya, M., Shea, M. J., Albrecht, U., Behringer, R. R., and Bradley, A. (1999) *Nat. Genet.* **22,** 361–365
12. van Amerongen, R., and Berns, A. (2006) *Trends Genet.* **22,** 678–689
13. Takada, S., Stark, K. L., Shea, M. J., Vassileva, G., McMahon, J. A., and McMahon, A. P. (1994) *Genes Dev.* **8,** 174–189
14. Yoshikawa, Y., Fujimori, T., McMahon, A. P., and Takada, S. (1997) *Dev. Biol.* **183,** 234–242
15. Saburi, S., and McNeill, H. (2005) *Curr. Opin. Cell Biol.* **17,** 482–488
16. Seifert, J. R., and Mlodzik, M. (2007) *Nat. Rev. Genet.* **8,** 126–138
17. Wang, Y., and Nathans, J. (2007) *Development* **134,** 647–658
18. Zallen, J. A. (2007) *Cell* **129,** 1051–1063
19. Simons, M., and Mlodzik, M. (2008) *Annu. Rev. Genet.* **42,** 517–540
20. Hamblet, N. S., Lijam, N., Ruiz-Lozano, P., Wang, J., Yang, Y., Luo, Z., Mei, L., Chien, K. R., Sussman, D. J., and Wynshaw-Boris, A. (2002) *Development* **129,** 5827–5838
21. Wallingford, J. B., and Harland, R. M. (2002) *Development* **129,** 5815–5825
22. Wang, J., Mark, S., Zhang, X., Qian, D., Yoo, S. J., Radde-Gallwitz, K., Zhang, Y., Lin, X., Collazo, A., Wynshaw-Boris, A., and Chen, P. (2005) *Nat. Genet.* **37,** 980–985
23. Wang, J., Hamblet, N. S., Mark, S., Dickinson, M. E., Brinkman, B. C., Segil, N., Fraser, S. E., Chen, P., Wallingford, J. B., and Wynshaw-Boris, A. (2006) *Development* **133,** 1767–1778
24. Etheridge, S. L., Ray, S., Li, S., Hamblet, N. S., Lijam, N., Tsang, M., Greer, J., Kardos, N., Wang, J., Sussman, D. J., Chen, P., and Wynshaw-Boris, A. (2008) *PLoS Genet.* **4,** e1000259
25. Cheyette, B. N., Waxman, J. S., Miller, J. R., Takemaru, K., Sheldahl, L. C., Khlebtsova, N., Fox, E. P., Earnest, T., and Moon, R. T. (2002) *Dev. Cell* **2,** 449–461
26. Katoh, M., and Katoh, M. (2003) *Int. J. Oncol.* **22,** 907–913
27. Zhang, L., Zhou, H., Su, Y., Sun, Z., Zhang, H., Zhang, L., Zhang, Y., Ning, Y., Chen, Y. G., and Meng, A. (2004) *Science* **306,** 114–117
28. Waxman, J. S., Hocking, A. M., Stoick, C. L., and Moon, R. T. (2004) *Development* **131,** 5909–5921
29. Zhang, L., Gao, X., Wen, J., Ning, Y., and Chen, Y. G. (2006) *J. Biol. Chem.* **281,** 8607–8612
30. Fisher, D. A., Kivimäe, S., Hoshino, J., Suriben, R., Martin, P. M., Baxter, N., and Cheyette, B. N. (2006) *Dev. Dyn.* **235,** 2620–2630
31. Gao, X., Wen, J., Zhang, L., Li, X., Ning, Y., Meng, A., and Chen, Y. G. (2008) *J. Biol. Chem.* **283,** 35679–35688
32. Gloy, J., Hikasa, H., and Sokol, S. Y. (2002) *Nat. Cell Biol.* **4,** 351–357
33. Su, Y., Zhang, L., Gao, X., Meng, F., Wen, J., Zhou, H., Meng, A., and Chen, Y. G. (2007) *FASEB J.* **21,** 682–690
34. Jiang, X., Tan, J., Li, J., Kivimäe, S., Yang, X., Zhuang, L., Lee, P. L., Chan, M. T., Stanton, L. W., Liu, E. T., Cheyette, B. N., and Yu, Q. (2008) *Cancer Cell* **13,** 529–541
35. Yau, T. O., Chan, C. Y., Chan, K. L., Lee, M. F., Wong, C. M., Fan, S. T., and Ng, I. O. (2005) *Oncogene* **24,** 1607–1614
36. Yang, X., Li, C., Xu, X., and Deng, C. (1998) *Proc. Natl. Acad. Sci. U.S.A.* **95,** 3667–3672
37. Tessarollo, L. (2001) *Methods Mol. Biol.* **158,** 47–63
38. Kuczuk, M. H., and Scott, W. J., Jr. (1984) *Teratology* **29,** 427–435
39. Nagy, A. (2003) *Manipulating the Mouse Embryo: A Laboratory Manual*, 3rd Ed., pp. 371–374, 630–673, Cold Spring Harbor Laboratory, Cold Spring Harbor, NY
40. Jho, E. H., Zhang, T., Domon, C., Joo, C. K., Freund, J. N., and Costantini, F. (2002) *Mol. Cell. Biol.* **22,** 1172–1183
41. Zhao, J., Ding, J., Li, Y., Ren, K., Sha, J., Zhu, M., and Gao, X. (2009) *Hum. Mol. Genet.* **18,** 3090–3097
42. Yi, H., Yu, X., Gao, P., Wang, Y., Baek, S. H., Chen, X., Kim, H. L., Subjeck, J. R., and Wang, X. Y. (2009) *Blood* **113,** 5819–5828
43. Benard, V., Bohl, B. P., and Bokoch, G. M. (1999) *J. Biol. Chem.* **274,** 13198–13204
44. Yamaguchi, T. P., Bradley, A., McMahon, A. P., and Jones, S. (1999) *Development* **126,** 1211–1223
45. Kibar, Z., Vogan, K. J., Groulx, N., Justice, M. J., Underhill, D. A., and Gros, P. (2001) *Nat. Genet.* **28,** 251–255
46. Haraguchi, R., Motoyama, J., Sasaki, H., Satoh, Y., Miyagawa, S., Nakagata, N., Moon, A., and Yamada, G. (2007) *Development* **134,** 525–533
47. Yamaguchi, T. P., Takada, S., Yoshikawa, Y., Wu, N., and McMahon, A. P. (1999) *Genes Dev.* **13,** 3185–3190
48. Galceran, J., Fariñas, I., Depew, M. J., Clevers, H., and Grosschedl, R. (1999) *Genes Dev.* **13,** 709–717
49. Philips, M. F., Dormans, J., Drummond, D., Schut, L., and Sutton, L. N. (1997) *Pediatr. Neurosurg.* **26,** 130–143
50. Sikandar, R., and Munim, S. (2009) *J. Pak. Med. Assoc.* **59,** 721–723
51. Singh, S. K., Singh, R. D., and Sharma, A. (2005) *Pediatr. Surg. Int.* **21,** 578–581
52. Saxén, L., and Sariola, H. (1987) *Pediatr. Nephrol.* **1,** 385–392
53. Michos, O. (2009) *Curr. Opin. Genet. Dev.* **19,** 484–490
54. Gygi, S. P., Rochon, Y., Franza, B. R., and Aebersold, R. (1999) *Mol. Cell. Biol.* **19,** 1720–1730
55. Merei, J. M. (2004) *Pediatr. Surg. Int.* **20,** 439–443
56. Axelrod, J. D., Miller, J. R., Shulman, J. M., Moon, R. T., and Perrimon, N. (1998) *Genes Dev.* **12,** 2610–2622
57. Boutros, M., Paricio, N., Strutt, D. I., and Mlodzik, M. (1998) *Cell* **94,** 109–118
58. Rothbächer, U., Laurent, M. N., Deardorff, M. A., Klein, P. S., Cho, K. W., and Fraser, S. E. (2000) *EMBO J.* **19,** 1010–1022
59. Wallingford, J. B., and Harland, R. M. (2001) *Development* **128,** 2581–2592
60. Schlessinger, K., Hall, A., and Tolwinski, N. (2009) *Genes Dev.* **23,** 265–277
61. Ybot-Gonzalez, P., Savery, D., Gerrelli, D., Signore, M., Mitchell, C. E., Faux, C. H., Greene, N. D., and Copp, A. J. (2007) *Development* **134,** 789–799
62. Hikasa, H., and Sokol, S. Y. (2004) *Development* **131,** 4725–4734
63. Brott, B. K., and Sokol, S. Y. (2005) *Dev. Cell* **8,** 703–715
64. Suriben, R., Kivimäe, S., Fisher, D. A., Moon, R. T., and Cheyette, B. N. (2009) *Nat. Genet.* **41,** 977–985